Appl. Phys. B 56, 84–93 (1993)

Applied Physics B Photophysics and Laser Chemistry

© Springer-Verlag 1993

Studies of Laser-Induced Cavitation and Tissue Ablation in Saline using a Fibre-Delivered Pulsed HF Laser

P. E. Dyer[1], M. E. Khosroshahi[1], and S. J. Tuft[2]

[1] Department of Applied Physics, The University of Hull, Hull, HU6 7RX, UK (Fax: +44-482/465606)
[2] Moorfields Eye Hospital, City Road, London, EC1V 2PD, UK

Received 30 July 1992/Accepted 20 October 1992

Abstract. We describe studies of the interaction of ~400 ns duration, fibre delivered, multiline (2.6–3.0 μm) HF-laser pulses with cornea and retina samples in saline. In this wavelength region water exhibits strong absorption (beam penetration depth ~1.6 μm) and laser heating leads to the creation of a hot, high pressure, vapour cavity (laser-induced cavitation) at the fibre tip. The dynamics of vapour cavity growth have been investigated experimentally using the laser shadowgraph technique and theoretically by employing an equivalent spherical cavity model for an incompressible liquid. Measurements of ablation rates and transient acoustic pressures for cornea ablation in saline, together with scanning electron microscope evaluation of irradiated samples are used to assess the damage range and mechanisms for this mid-IR laser in a strongly absorbing fluid.

PACS: 42.55.Em, 43.35.+d, 87.00

There is currently much interest in the use of pulsed ultraviolet (UV) and infrared (IR) lasers for tissue ablation [1–9]. In the IR, pulsed Er:YAG, Ho:YAG and HF lasers are particularly important as they operate at wavelengths where fibre delivery is efficient and tissues, by virtue of their water content, exhibit strong absorption restricting residual thermal damage to a relatively small zone [3–6, 10–12]. Whilst this is also true for certain excimer-laser wavelengths, e.g. KrF (248 mn) and XeCl (308 nm) [9], the use of deep-UV radiation for tissue ablation has unresolved issues associated with mutagenicity and toxicity [13] which are absent for the near-IR lasers.

We have recently reported studies of pulsed (~400 ns), multiline (2.6–3.0 μm), HF laser transmission in a fluoride glass fibre and have demonstrated that sharply defined incisions in tissue can be produced by ablation with this system [14]. However, as many medical applications involve a wet field we report here an extension of our studies to tissue ablation using the fibre-delivered HF laser in saline. Under these conditions, as Lin et al. [15] have recently shown for the Er:YAG laser, bubble growth is initiated at the fibre tip because of the strong absorption in water which leads to the creation of a hot, high-pressure vapour cavity (laser-induced cavitation). These bubbles exhibit complex dynamics and can act as transmissive cavities that greatly extend the effective beam penetration range for relatively long pulse IR lasers [15, 16]) i.e. comparable to the bubble growth time. Even in the absence of this effect, as would be the case with suitably short laser pulses, cavitation leads to energy being transported well beyond the laser beam penetration depth as a direct result of the bubble expansion following the pulse and large amplitude acoustic waves associated with bubble formation and decay. This may be advantageous in circumstances where it is desirable to achieve tissue modification or removal when a liquid layer intervenes and strongly attenuates the laser beam between the fibre tip and sample. However, such effects are undesirable under conditions where it is necessary to localize the interaction so as to minimize adjacent tissue damage [15].

Here we report quantitative studies of the dynamics of bubbles produced by the fibre-delivered HF laser in saline using pulsed dye-laser shadowgraphy [15–17]. The HF laser provides a well defined single pulse output of ~400 ns duration, considerably shorter than used in previous studies [15, 16]. Material removal rates and pressure transients produced by HF laser ablation of cornea samples have been measured for the fibre in contact with the sample in saline. Scanning electron microscopy (SEM) has been used to evaluate the ablation site for cornea, and estimates have been made of the fibre-sample spacing at which surface damage is induced in retina and in cornea samples.

1 Experimental Technique

A multiline HF laser emitting on 20 transitions spanning the wavelength range 2.67–2.96 μm was coupled into a short length (150 mm) of fluoride glass fibre (480 μm core diameter, Infrared Fibre Systems, MD, USA). The fibre carried the ~400 ns full-width at half-maximum (FWHM) HF laser pulse into a small saline bath via a sealed bushing in the wall of the vessel (Fig. 1). Fast photographic recording of

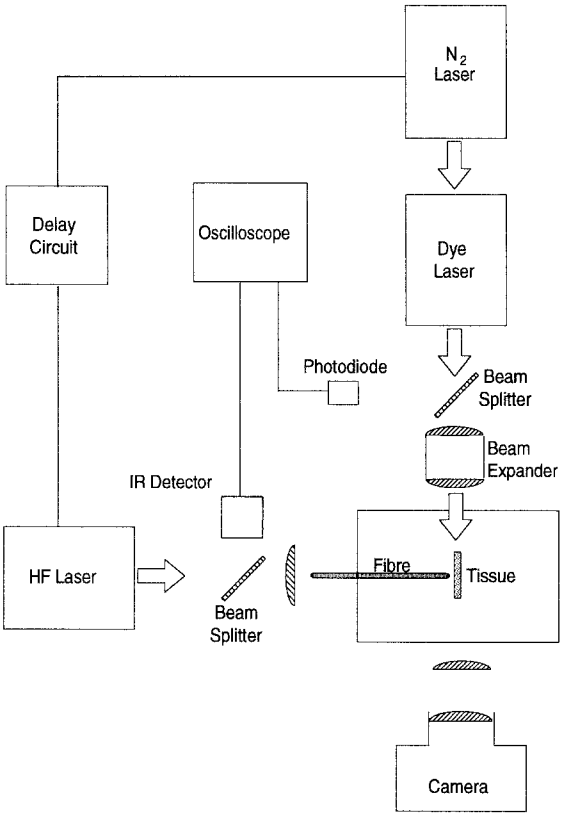

Fig. 1. Experimental arrangement

bubbles produced in the vicinity of the fibre tip was implemented using the laser shadowgraph technique [15–17]. This used the output from a fibre-delivered N_2-pumped dye laser (4 ns pulse duration, wavelength $\cong$573 nm, rhodamine 6G) suitably expanded to provide a 13 mm diameter collimated beam traversing the liquid cell transverse to the fibre (Fig. 1). A polaroid camera was used to record the magnified ($\times$2.1) image of the laser illuminated fibre. An electronic pulse delay generator triggered by the HF laser pulse was used to vary the arrival time of the dye-laser pulse allowing a sequence of bubble pictures to be built up.

Pressure transients produced in tissue samples were recorded using a polyvinylidene fluoride (PVDF) film piezoelectric transducer (9 µm thick). The PVDF film was mounted onto a 4 mm thick perspex impedance matching stub and a thin mylar film was bonded to its front surface to avoid direct contact of its aluminized electrodes with saline. Tissue samples of cornea (sections $\sim$250–300 µm thick) or retina were mounted onto the front of the transducer under pressure using a suitable retaining frame. The electrical output from the transducer was taken to a 1 MΩ Tektronix plug-in amplifier providing a voltage response proportional to the normal force at the transducer [18]. The overall response time for the transducer system was estimated to be $\sim$ 4 ns. Samples of cornea or retina were obtained from freshly enucleated bovine eyes and were stored in saline prior to use. Corneal samples were exposed on their epithelial side with the fibre oriented normal to and at various distances

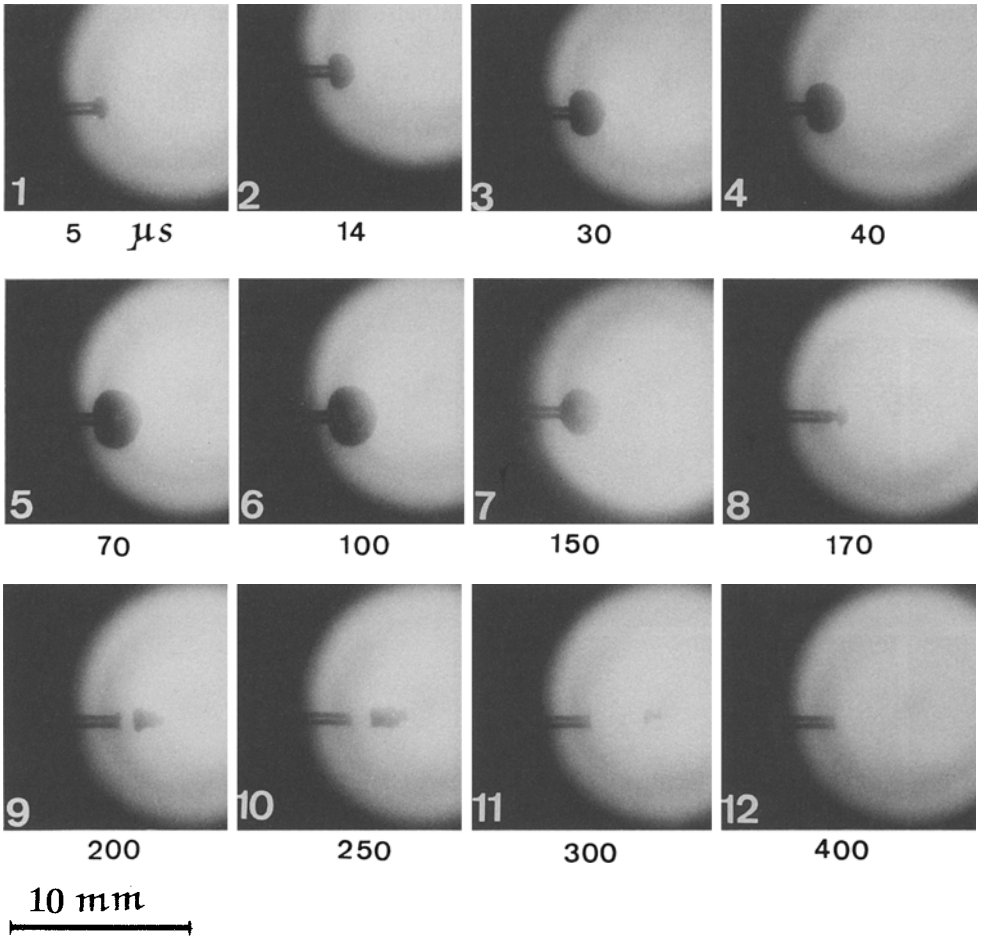

Fig. 2. Sequence of bubble shadowgraphs obtained over the time period 5–400 µs for fibre-delivered HF-laser pulse (fibre in saline; exit fluence 5.5 J cm^{-2}). Between frames 11 and 12 the bubble fragments produce many small bubbles although this is difficult to resolve in this figure

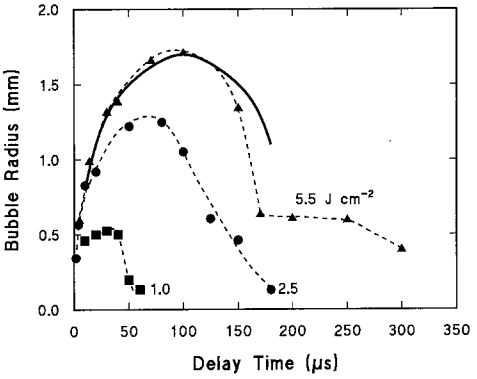

Fig. 3. Bubble radius as a function of time for exit fluences from the fibre of 1, 2.5 and 5.5 J cm^{-2}. The broken lines are fits to the data to guide the eye. The solid line is the calculated bubble radius suitably scaled to have the same maximum radius as the experimental value at 5.5 J cm^{-2}

from the surface. Following laser exposure the depth of tissue removed was measured using a high-resolution optical microscope (Olympus BHM, $\pm 2\,\mu$m depth resolution). For SEM evaluation the tissues were fixed in glutaraldehyde-formaldehyde (GF fixative) and dried using a critical point drying apparatus to minimize structural deformation or collapse.

2 Experimental Results

Shadowgraphs were recorded at various delay times with respect to the HF laser pulse for several exit fluences from the fibre and for various fibre–tissue sample geometries. Figure 2 shows a sequence of photographs obtained at a fibre exit fluence of 5.5 J cm^{-2} for the simplest configuration – free saline and no tissue sample. It is evident from these photographs that a vapour bubble expands from the fibre tip so as to form a cavity that is initially approximately spherical but somewhat flattened towards the fibre side. The bubble

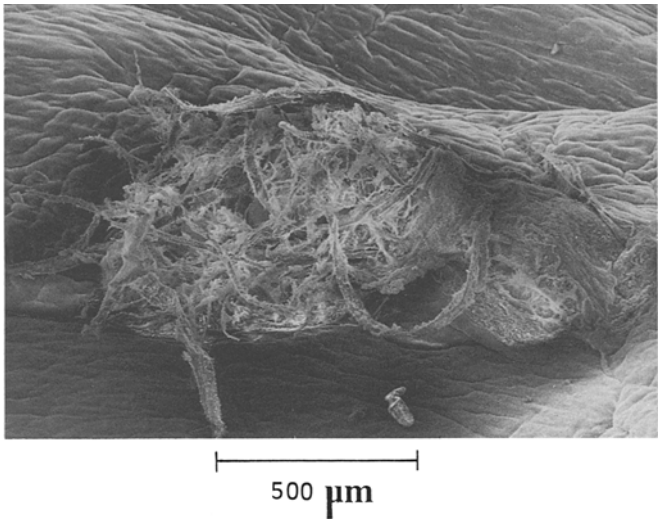

Fig. 5. Surface of cornea following exposure to 20 pulses from HF laser with fibre tip located ~200 μm from the sample in saline (fluence, 5 J cm^{-2})

reaches a maximum diameter of ~3.4 mm transverse to the fibre and then collapses producing a distinctly non-spherical cavity beyond ~150 μs. This ultimately moves away from the fibre tip at a velocity of ~10^5 mm s^{-1} for the front of the bubble. At a distance of about 3 mm from the fibre tip close inspection of frame 11 and 12 in Fig. 2e reveals that the bubble apparently breaks up forming many smaller-diameter bubbles. A similar behaviour has been reported by Lin et al. [15] for a multiple pulse Er:YAG laser delivered using a fibre in saline.

In Fig. 3 plots of the transverse radius of the bubble, r, are shown as a function of time for fibre exit fluences of 1, 2.5 and 5.5 J cm^{-2}. In each case the bubble reaches a maximum size and then collapses; the maximum bubble size and the time scale for growth and collapse decrease as the fluence decreases. The bubbles in each example appeared to become unstable in the final stage of collapse, dissipating

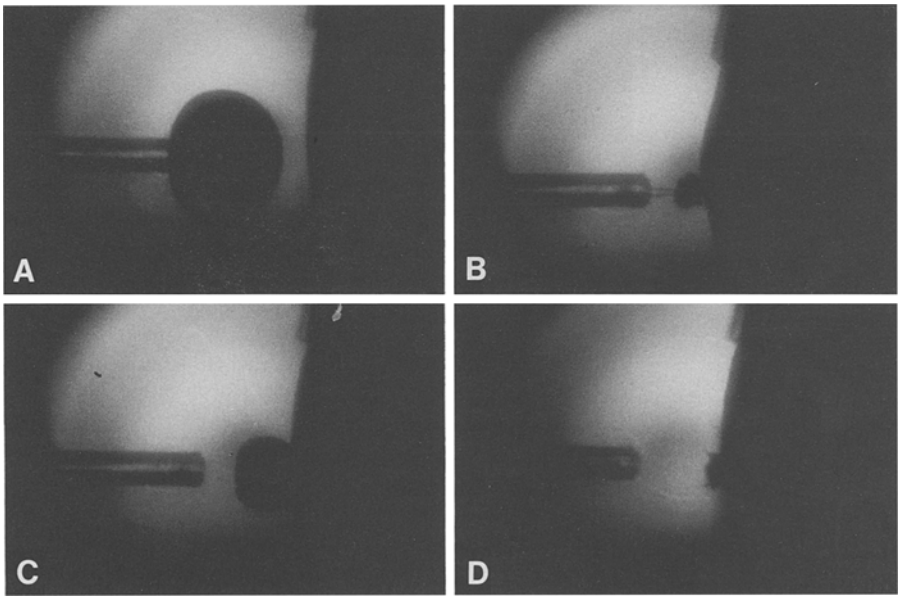

Fig. 4A–D. Bubble sequence for fibre in saline with tip positioned 2.5 mm from a cornea sample. **A** –100 μs, **B** –300 μs, **C** –400 μs, **D** –480 μs (fluence 5 J cm^{-2})

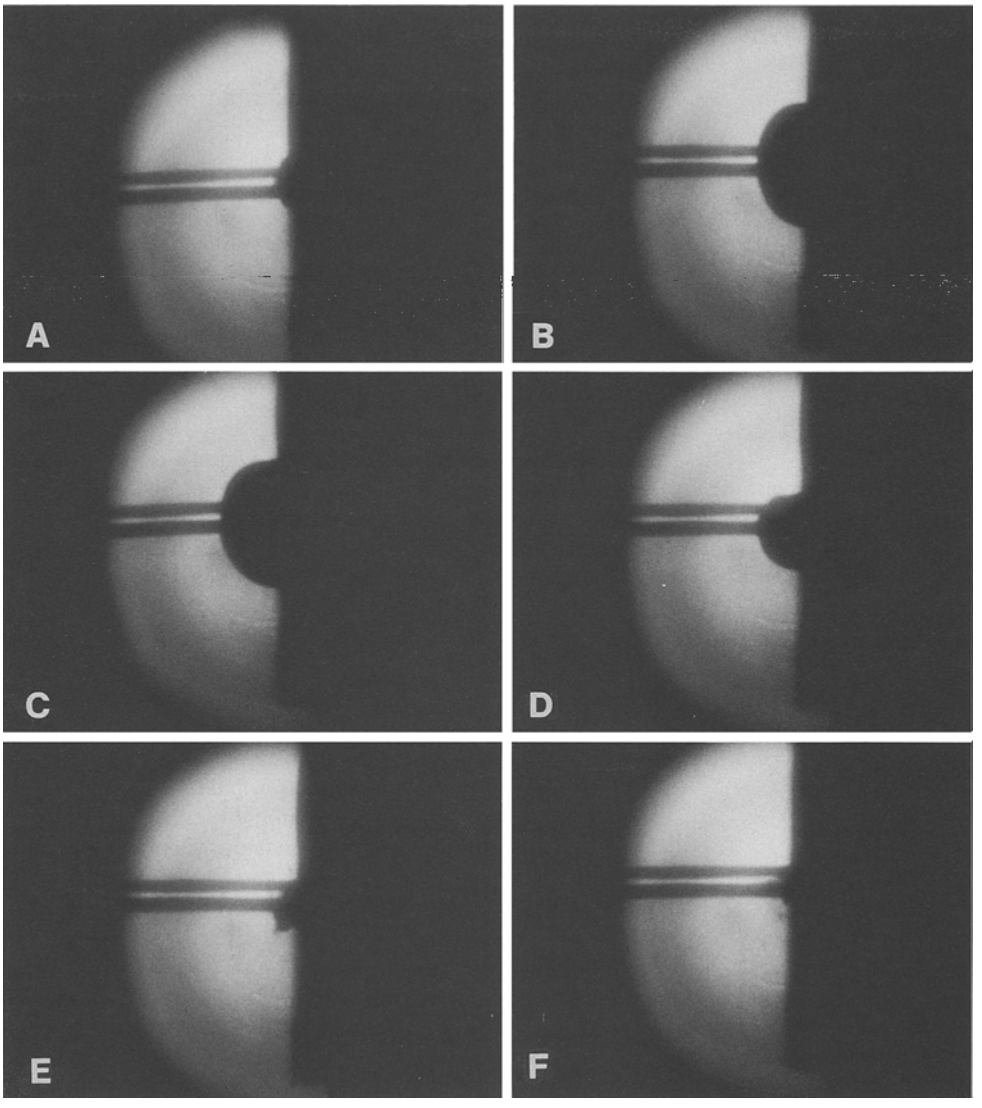

Fig. 6A–F. Shadowgraphs of fibre delivered HF laser in saline with fibre touching the cornea surface. **A** – 10 µs, **B** – 70 µs, **C** – 150 µs, **D** – 250 µs, **E** – 300 µs, **F** – 400 µs (fluence 4.5 J cm^{-2})

through the generation of minute bubbles. The threshold exit fluence for the onset of an observable vapour cavity using the shadowgraph technique was found to be $\sim$0.6 J cm^{-2}; However, only for fluences exceeding about 2 J cm^{-2} did bubbles detach from the fibre tip and gain a significant forward velocity component.

In Fig. 4 a sequence of shadowgraphs is shown for the fibre operating at an exit fluence of 5 J cm^{-2} with its tip located 2.5 mm away from a cornea sample. Notable in this sequence is the apparent "jetting" behaviour of the cavity in the frame at $\sim$300 µs and subsequent rexpansion and then collapse at times of 400 µs and 480 µs, respectively. SEM and optical microscope inspection of corneal samples located at various distances, d, from the fibre tip revealed that observable damage of the sample only occurred for $d \leq 250$ µm for multishot exposure at fluences of 5 J cm^{-2}. Figure 5 shows an SEM of the corneal surface damage that resulted following 20 pulses at an exit fluence of 5 J cm^{-2} with the fibre tip located $\sim$200 µm from the surface. There is extensive damage in the form of disruption and distortion of stromal collagen fibrils over a zone exceeding 1 mm in diameter. As will be discussed later, even at this small separation the HF laser beam cannot penetrate to the sample surface so that the damage is either produced by the expanding vapour bubble or is a result of mechanical disruption produced by an intense acoustic wave or possibly a combination of these effects. Similar measurements for retina showed that local surface disruption could be produced with the fibre tip at much larger distances from the sample (e.g. out to $\sim$2 mm at 4.5 J cm^{-2}), as a result of the greater sensitivity of this tissue to damage. In this context it is of interest to note that for cornea endothelium the damage range of optical breakdown plasmas produced by picosecond [19] and nanosecond [20] YAG-laser pulses is considerably larger ($\sim$800 µm estimated for similar pulse energies) than observed here, where the epthelial side was exposed. This is most probably because of the greater sensitivity of cornea endothelium to damage although it is also possible that the presence of the fibre modifies bubble collapse in a way that reduces the effects of jetting on the surface.

Shadowgraphs recorded for the fibre in intimate contact with a cornea sample in saline are shown in Fig. 6 (exit fluence 4.5 J cm^{-2}). At 10 µs a small hemispherical cavity has already developed around the fibre tip as a result of the ablation products being forced between the core and jacket region of the fibre face into the surrounding liquid.

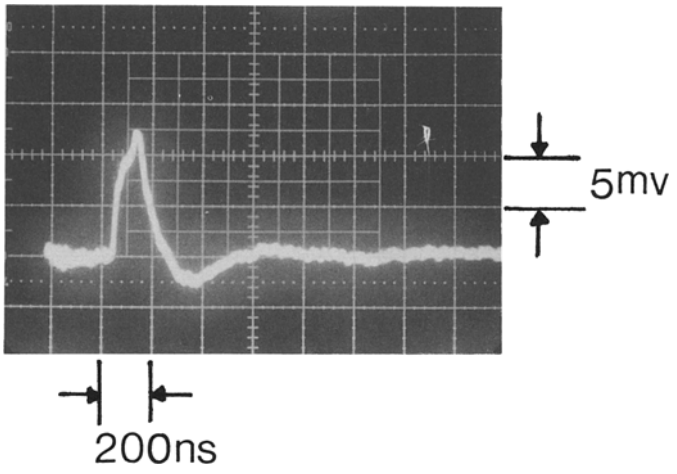

Fig. 7. Transient pressure pulse produced by ablation of cornea with contacted fibre in saline (fluence, 2.5 J cm^{-2}). The start of the trace is triggered by the HF-laser pulse

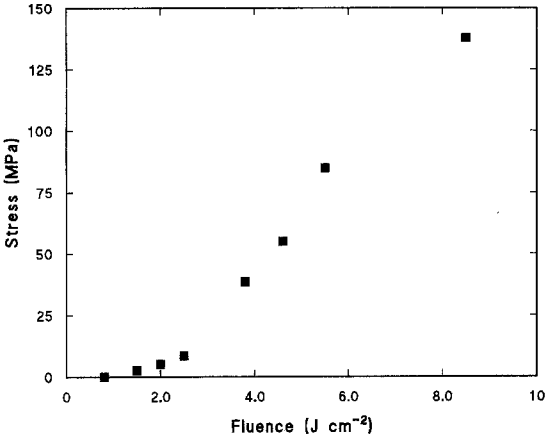

Fig. 8. Peak stress deduced from the photoacoustic transducer as a function of fluence for HF-laser ablation of cornea. Contacted fibre in saline

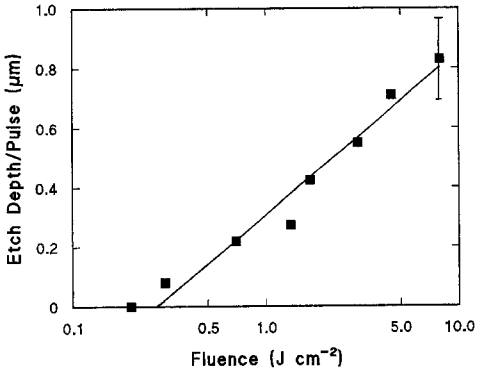

Fig. 9. Average etch-depth per pulse for cornea with contacted fibre in saline as a function of HF-laser fluence

This hemispherical expansion continues up to ~250 μs and then collapse occurs, the bubble ultimately disappearing at ~400 μs. For fluences exceeding ~5 J cm^{-2} with the contacted fibre, stress levels associated with cavitation were sufficiently large to cause fracture and break-up of the

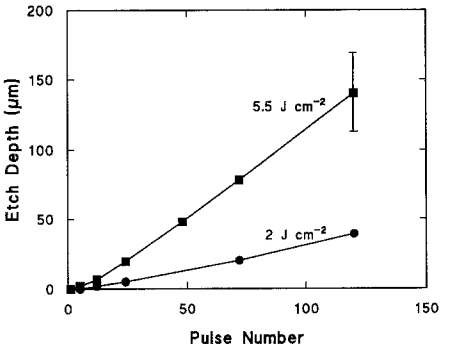

Fig. 10. Etch-depth as a function of number of ablating pulses at exit fluences of 2 and 5.5 J cm^{-2} with contacted fibre

acrylate jacket of the fibre in the vicinity of its tip. This effect was not observed for ablation in air [14].

Measurements of the transient pressure pulse accompanying ablation for the contacted fibre ($d = 0$) were made for a ~300 μm thick section of cornea mounted on the PVDF piezoelectric transducer. The transducer output shown in Fig. 7 for an exit fluence of 2.5 J cm^{-2} exhibited a fast rise time (~80 ns), a duration of ~200 ns (FWHM) and some ringing following the main pulse. The oscilloscope trace was triggered by the laser pulse using an IR photodiode and it was observed that the delay between pulses decreased as the fluence was raised. This delay has a fixed component set by the acoustic transit time in the sample (neglecting shock effects) and a component that depends on when ablation commences during the laser pulse. It can thus be deduced that ablation occurs at earlier times as the fluence is increased.

The peak output voltage from the PVDF transducer can be converted to a corresponding normal force [18] and hence to a pressure if the area of influence of the acoustic pulse can be defined. For this purpose we assume that a plane acoustic wave propagates between the tissue surface and transducer and take the area as that of the fibre core. It should be noted, however, that this is a relatively poor assumption in the present case because the transducer lies beyond the near-field range, Z_R. This is given by [18]

$$Z_R = a^2/\lambda,$$

where a is the fibre core radius and λ is the characteristic acoustic wavelength generated in the interaction. Taking $a = 240\,\mu\text{m}$, $\lambda \cong 2c\Delta t$, where Δt is the width of the pressure pulse (Fig. 7) and c the sound speed for bulk longitudinal waves in the tissue ($c \cong 1.5 \times 10^3\,\text{ms}^{-1}$), $Z_R \cong 100\,\mu\text{m}$. This is considerably smaller than the tissue sample thickness (~300 μm) so that significant "edge" effects will occur, i.e. three-dimensional expansion effects cannot strictly be neglected. This transition to nonplanar propagation may explain why a rarefaction component develops on the pressure pulse.

In spite of this limitation pressure amplitudes were calculated assuming plane wave propagation and the resulting peak pressure derived in this way is shown in Fig. 8 as a function of fluence. It is clear that large stresses are generated for the contacted fibre geometry, values exceeding 10^8 Pa being recorded for exit fluences above ~7 J cm^{-2}. On longer timescales than shown in Fig. 7 the transducer output exhibited complex voltage oscillations, probably mainly arising

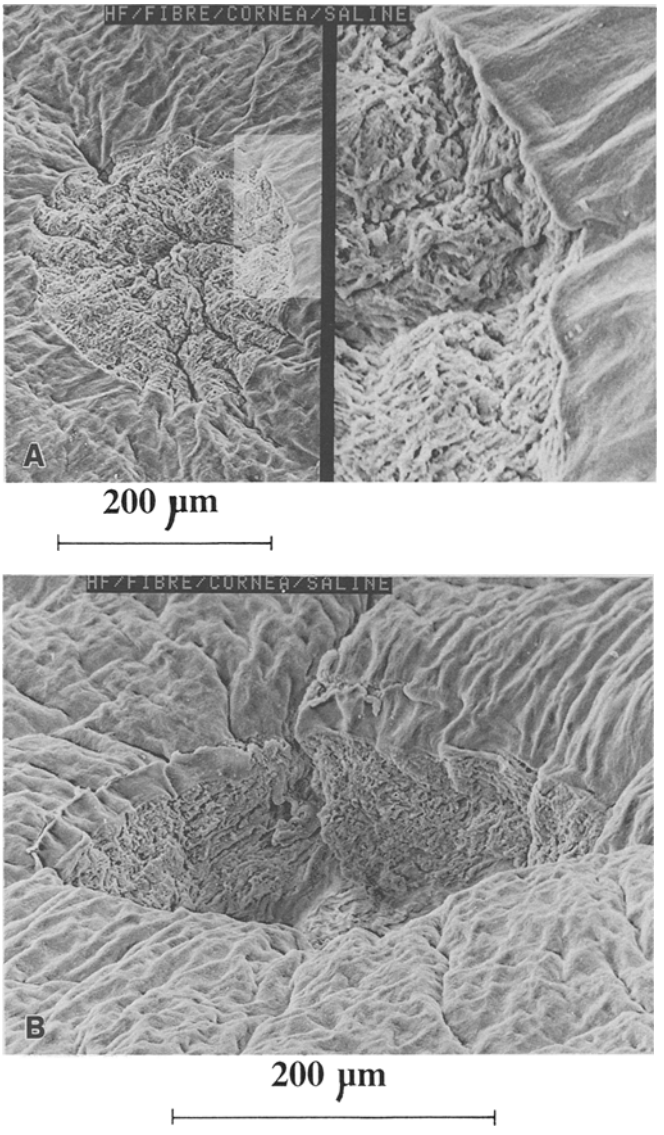

Fig. 11A, B. Scanning electron micrographs of cornea ablated using contacted fibre in saline at 5 J cm^{-2}. **A** 1 pulse; **B** 100 pulses

from acoustic reflections at the many near-lying interfaces in the liquid cell. These effects unfortunately prevented an unambiguous identification of pressure pulses that may have been associated with the long-term expansion and collapse phase of the bubble.

Ablation rates for cornea with the contacted fibre in saline are shown in Fig. 9 as a function of fluence. An approximate threshold for ablation of $\sim$0.4 J cm^{-2} was obtained from the log-linear plot, which is similar to that measured for an air-based fibre [14]. The removal rates are much lower, however, than in air particularly at high fluence and remain $\lesssim$1 µm per pulse for fluencces up to $\sim$9 J cm^{-2}. Interestingly, measurements of the ablation depth as a function of pulse number for several fluences showed that the removal rate per pulse was essentially constant at least for the modest ablation depths involved (Fig. 10).

SEM photographs of the ablation site for the contacted fibre are shown in Figs. 11a, b for exposure at 5 J cm^{-2} for 1 and 100 pulses. The interaction zone is significantly smaller in diameter than the fibre core, possibly because of some fluence nonuniformity at the fibre exit surface. It is evident that the ablated surface is essentially free of debris and that with 100 pulses a sharply defined incision is produced that clearly penetrates the epithelium and superficial stroma. This behaviour is closely similar to that for an air-based contacted fibre [14] but is in sharp distinction to the damage produced when the fibre is moved only a small distance from the surface (d = 200 µm, e.g. Fig. 5). This suggests that the interaction mechanism responsible for "damage" is significantly different in the two cases.

3 Analysis

The dynamics of laser-induced cavitation bubbles have been extensively studied and analysed for cases where a focused laser produces spherical bubbles either in free liquid or liquid in the vicinity of a plane solid or air boundary [21]. For cavitation initiated by a fibre-delivered laser the situation is more complicated because aspherical growth is promoted by the planar geometry of the initial vapour cavity formed at the fibre tip and by the perturbing influence of the fibre during "bubble" growth. This is evident from Fig. 2 where the vapour bubble is observed to be somewhat flattened in the direction parallel to the fibre axis. Given the lack of a readily applicable theory for aspherical growth [21], an analysis based on a spherical-cavity model is retained here by assuming that it is justifiable to define an equivalent spherical radius for the bubble.

In Fig. 3 the bubble radius (transverse to the fibre axis) – time plot is seen to be approximately symmetrical and is similar to the behaviour observed for the growth and collapse of spherical bubbles [21, 22]. The characteristic collapse (and growth) time for gas filled spherial bubbles is given by [22]

$$\tau = 0.91\, R_m(\varrho/P_0)^{1/2}(1 + P_f/P_0)\,, \tag{1}$$

where R_m is the maximum bubble radius, ϱ is the liquid density, P_0 is the liquid pressure (atmospheric pressure as the hydrostatic contribution from the liquid is negligible), and P_f is the pressure in the fully expanded bubble. Estimates discussed below show $P_f/P_0 \lesssim 2.7 \times 10^{-2}$ so that τ is very close to that for collapse of an empty cavity), i.e. with $P_f = 0$.

At an exit fluence of 5.5 J cm^{-2} we obtain from Fig. 3 $\tau \cong 100$ µs so that with $P_0 = 10^5$ Pa, R_m is calculated from (1) to be 1.1 mm compared with $r_m \cong 1.7$ mm for the measured maximum transverse radius of the bubble. On this basis the effective radius is substantially lower than r_m which is not unreasonable given that the bubble is a flattened sphere into which the fibre protrudes. In addition, volume may be lost due to liquid that penetrates into the axial regions of the bubble but is not detected in the shadowgraph which only delineates the cavity boundary.

The growth of a spherical vapour cavity can be described by the following equation which can be derived from energy considerations [22]:

$$\varrho\dot{R}^2 = \frac{2P_i}{3(\gamma-1)}[(R_i/R)^3 - (R_i/R)^{3\gamma}] - \frac{2P_0}{3}[1 - (R_i/R)^3]\,. \tag{2}$$

Here R is the radius of the cavity and $\dot{R}$ the corresponding wall velocity. At $t = 0$, the cavity velocity satisfies $\dot{R} = 0$, $R = R_i$ and the vapour pressure is P_i. It is assumed that in the subsequent expansion the vapour obeys an ideal adiabatic gas law of the form $PV^\gamma =$ constant, where $\gamma \cong 4/3$ is the ratio of specific heats. In deriving (2) it is assumed that surface tension and viscous effects are negligible and that the liquid is incompressible. The assumption of incompressibility leads to the cavity wall velocity being zero at $t = 0$ and only increasing slowly with time at early stages of the expansion. This follows because the corresponding acoustic velocity in the liquid is infinite in this approximation and the gas cavity cannot accelerate a finite mass of liquid instantaneously. Whilst this treatment is adequate for analysing the long-term expansion and contraction phase of bubbles it is necessary, as will be seen later, to take compressibility into account when estimating acoustic pressure levels produced in the initial stages of the laser interaction.

To evaluate (2) we take $P_i = 8.5 \times 10^7$ Pa based on the peak stress estimated from the photoacoustic transducer at 5.5 J cm^{-2} (Fig. 8) and $P_0 = 10^5$ Pa. The resulting variation in velocity with radius is shown in Fig. 12 where $(3\varrho/2P_0)^{1/2}\dot{R}$ is plotted as a function of R/R_i. In this case the maximum expansion ratio is $R_m/R_i = 13.3$ which with $R_m = 1.1$ mm gives $R_i = 8.2 \times 10^{-2}$ mm for the radius of the initial (equivalent) spherical cavity. Assuming no dissolved air enters from the liquid, the pressure P_f, in the fully expanded cavity can be estimated using $P_f = P_i(R_i/R_m)^{3\gamma}$, to be 2.7×10^3 Pa. This corresponds to $P_f/P_0 = 2.7 \times 10^{-2}$ indicating that the final pressure is substantially lower than the local hydrostatic pressure. A corresponding R–t plot derived by integrating (2) numerically is shown for comparison with the experimental data obtained at 5.5 J cm^{-2} in Fig. 3.

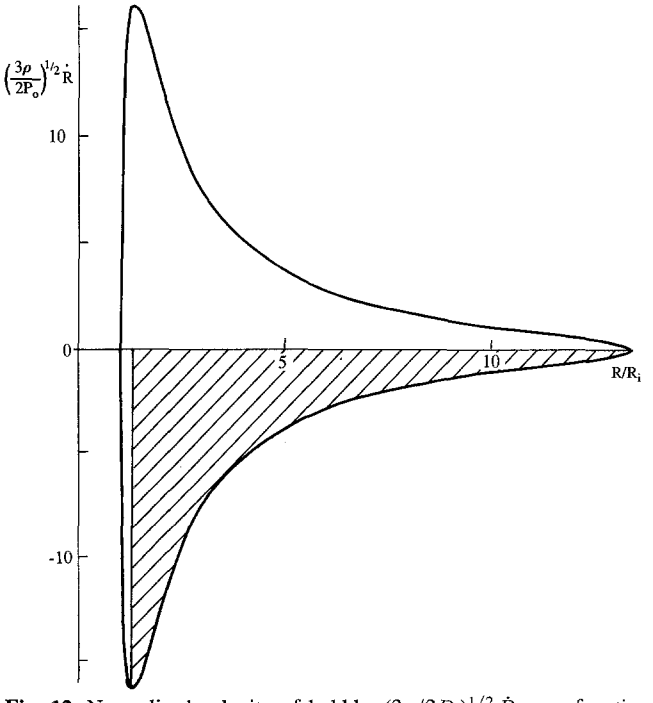

Fig. 12. Normalised velocity of bubble, $(3\varrho/2P_0)^{1/2}\dot{R}$, as a function of R/R_i; for this calculation the initial radius $R_i = 8.2 \times 10^{-2}$ mm, the initial pressure $P_i = 8.5 \times 10^7$ Pa, $\gamma = 1.33$ and $P_0 = 10^5$ Pa. In the shaded region the liquid accelerates the wall of the vapour cavity

The calculated value for R has been scaled by a factor of r_m/R_m to normalize the data at the maximum radius allowing direct comparison whith transverse radius obtained experimentally. It can be seen that this equivalent spherical model gives surprisingly good agreement with the experimental results in the expansion phase, especially given the considerable simplifications involved. For the collapse the agreement is less good particularly beyond ~150 μs, the time at which the bubble becomes aspherical and develops a significant forward velocity component (Fig. 2). For $170 \lesssim t \lesssim 300$ μs it remains approximately constant in its transverse width and acquires a distinctly non-spherical shape, ultimately fragmenting at $t \cong 300$ μs to produce many small bubbles.

The apparent instability of the cavity during the collapse phase is consistent with the onset of the Rayleigh-Taylor instability for a *curved* liquid-gas interface [22]. Under these conditions boundary instability may occur when a dense fluid accelerates a less dense fluid (shaded region in Fig. 12) in contrast to a planar interface where the reverse applies. The bubble instability is presumably accentuated by the presence of the fibre and contrasts to laser induced cavities produced in a free liquid which can remain stable and undergo multiple expansion and contraction phases [23]. It is also of interest that above some critical fluence the bubble develops a significant forward velocity component during the collapse phase, a feature that appears to be peculiar to cavitation produced at a fibre tip [15]. This differs from cavities produced near solid boundaries of large extent which are generally observed to be attracted towards the boundary [22]. An understanding of this behaviour is lacking at present and requires further theoretical work.

At its maximum radius the velocity of the bubble wall and hence of the liquid falls to zero and from the work done on the liquid the potential energy E_0 of the cavity is found to be:

$$E_0 = 4\pi R_m^3 P_0/3 . \tag{3}$$

Assuming that the R_m is given by the equivalent spherical radius we then obtain $E_0 \cong 0.55$ mJ at an exit fluence of 5.5 J cm^{-2} when $R_m = 1.1$ mm. This is much lower than the energy of 9.9 mJ delivered to the liquid by the 480 μm core diameter fibre at this fluence. Similar findings have been reported by Teng et al. [24] who attribute this to various losses in the expansion phase. The deficit, however, can largely be accounted for by the substantial difference in enthalpy for water (~2500 J gm^{-2}) in the (expanded) vapour and the liquid phase although there are small contributions due to heat conduction loss to the fibre tip and energy radiated as acoustic waves. The latter are evaluated in the following sections.

4 Laser–Liquid Interaction at the Fibre Tip

Water exhibits strong absorption at the wavelengths emitted by the multiline HF laser and as a result energy is deposited in a very shallow region adjacent to the fibre tip. For low fluences the heated depth, neglecting thermal conduction, is $\alpha^{-1} \cong 1.6$ μm, where α is the average absorption coefficient ($\alpha \cong 6 \times 10^3$ cm^{-1}). Heating will lead to thermoelastic stress

being generated due the water expanding and if the fluence is high enough boiling can take place, i.e. if $T \geq 373\,\mathrm{K}$ for $P_0 \cong 10^5\,\mathrm{Pa}$. Under conditions where the characteristic laser pulse duration, τ_L, is much longer than the timescale, $(\alpha c)^{-1}$, for an acoustic wave to travel across the heated zone, the peak thermoelastic stress can be shown to be [18]:

$$\sigma_T \cong f \Gamma I_0 / c$$

Here I_0 is the peak laser irradiance, $\Gamma \cong 0.1$ is the Gruneisen constant for water [18] and $f \lesssim 0.5$ is a factor that depends on the precise laser pulse shape. For the present conditions estimates give $f = 0.1$ so that for $I_0 \lesssim 10^6\,\mathrm{W\,cm^{-2}}$, $\sigma_T \lesssim 7 \times 10^4\,\mathrm{Pa}$, i.e. the thermoelastic stress is relatively small. This is because stress relaxation by the propagation of an acoustic wave across the heated zone occurs on a timescale ($\sim 0.6\,\mathrm{ns}$) that is much smaller than τ_L ($\lesssim 400\,\mathrm{ns}$).

In principle, boiling of the heated water layer can take place once its temperature exceeds $\sim 373\,\mathrm{K}$ under conditions where the local pressure in the liquid is $\sim 10^5\,\mathrm{Pa}$. However, because of the strongly nonequilibrium nature of the interaction we postulate that substantial superheating occurs, i.e. the temperature exceeds $T(P_v) = 373\,\mathrm{K}$, where $P_v \cong 10^5\,\mathrm{Pa}$ is the vapour pressure that exists under equilibrium conditions. This can be justified by noting that heat extraction by bubble growth from microscopic vapour pockets can only take place if the temperature and vapour pressure is sufficiently high to overcome surface tension effects [25]. In addition, even if bubble growth is initiated, the large difference in volume between the liquid and vapour below the critical point together with the finite bubble growth velocity will limit the maximum rate at which energy can be transferred to the vapour. If this falls below the rate at which energy is input from the laser then the liquid temperature will continue to increase, i.e. superheating occurs. On this basis we argue that the liquid is heated at approximately constant pressure ($\sim 10^5\,\mathrm{Pa}$) to the critical temperature ($T_c = 647\,\mathrm{K}$) at which point distinction between liquid and vapour is lost. The pressure then increases sharply and growth of a vapour cavity can take place.

An estimate of the threshold fluence, F_T, for attaining the critical temperature can be obtained from

$$F_T \alpha' = \Delta H_v\,,$$

where α' is the mass absorption coefficient of water for the multiline HF laser and ΔH_v is the enthalpy difference between water at room temperature and the critical point ($\sim 2000\,\mathrm{J\,gm^{-1}}$). If $\alpha' = \alpha/\varrho$ is assumed to be constant with a value of approximately $6 \times 10^3\,\mathrm{cm^2\,gm^{-1}}$ derived from available room temperature data [26] suitably weighted for the laser spectrum, then $F_T = 0.33\,\mathrm{J\,cm^{-2}}$. A correction to account for heat loss by conduction to the fibre tip can be estimated from

$$F_f = S(T_c - T_R)(4D\tau_L)^{1/2}\,,$$

where $S \cong 3.7\,\mathrm{J\,cm^{-3}\,K^{-1}}$ is the mean volume heat capacity and $D \cong 1.8 \times 10^{-3}\,\mathrm{cm\,s^{-1}}$ is the mean thermal diffusivity of the fluoride glass fibre [271. This gives $F_f \cong 0.07\,\mathrm{J\,cm^{-2}}$ and raises the threshold fluence to $\sim 0.4\,\mathrm{J\,cm^{-2}}$. This is considerably lower than the fluence at which a detectable cavity is revealed by the shadowgraph technique, i.e. around $0.6\,\mathrm{J\,cm^{-2}}$. It is noted, however, that this calculated "threshold" corresponds to the attainment of the critical temperature at the water surface in contact with the fibre tip; substantially higher fluences are probably necessary to ablate a sufficiently large volume to promote bubble growth.

5 Photoacoustic Response

Photoacoustic measurements made for the fibre contacted to the tissue surface show that detectable pressures occur for exit fluences from the fibre exceeding $\sim 0.9\,\mathrm{J\,cm^{-2}}$ and that the peak pressure increases steadily above this value (Fig. 8). An estimate of the peak pressure generated under these conditions can be made as follows; we assume that ablation commences at that time, t_a, during the pulse when the net fluence delivered to the surface reaches the threshold value and that the ablation products expand by compressing the tissue surface. If as a result of ablation a layer of material of thickness Δx is converted to an ideal gas, the pressure P is found using

$$P = (\gamma - 1)\Delta F / \Delta x\,, \tag{4}$$

where ΔF is the fluence delivered to the layer in a characteristic time $\Delta\tau$ for pressure release to occur by expansion. $\Delta\tau$ is estimated as

$$\Delta\tau = \Delta x / u = \Delta x\, \varrho c / P\,, \tag{5}$$

where u is the expansion rate of the gas cavity given by the local particle velocity produced in the confining tissue by the passage of a plane acoustic wave of pressure P (shock effects are neglected and it is assumed that the fibre is incompressible). Then using $\Delta F = I(t_a)\Delta\tau$, where $I(t_a)$ is the laser irradiance at t_a, we obtain from (4) and (5):

$$P = [\varrho c I(t_a)(\gamma - 1)]^{1/2}\,. \tag{6}$$

It is implicitly assumed in deriving (6) that the peak pressure occurs at the inception of ablation. This is reasonable if the laser irradiance satisfies $I < I(t_a)$ for $t > t_a$, making the expression applicable to fast rising but finite duration (and monotonically decreasing) laser pulses.

A similar expression has been used by Zweig and Deutsch [28] to describe pressures generated in the excimer-laser ablation of polyimide in a liquid environment. In that case, provided ablation commences at a fixed time near the peak of the laser pulse, the pressure scales as $(F/\tau)^{1/2}$, where F is the fluence and τ the pulse duration. In the present experiments using a fast rise-time but relatively long duration laser pulse ($\sim 900\,\mathrm{ns}$ full duration) the pressure-fluence dependence is anticipated to be more complicated than $F^{1/2}$. This is because for fluences near to but exceeding the threshold, ablation will commence near the end of the pulse producing low pressures because $I(t_a)$ is low. As the fluence is raised ablation will progressively occur at earlier times in the pulse leading to an increase in pressure that depends not only on fluence but the detailed shape of the laser pulse. Ultimately at high fluence ablation will occur at a fixed time near the peak of the laser pulse and the pressure will exhibit an $E^{1/2}$ dependence [28]. This behaviour at least qualitatively can be used to explain the form of the

variation observed in Fig. 8 where the pressure increases quite rapidly with fluence near threshold but starts to level out at high fluences. The fast rising form of the pressure transient (Fig. 7) and observation that the appearance of the pressure pulse moves to earlier times with increasing fluence also provides qualitative support for the model.

The peak pressures predicted using (6) are in broad agreement with the experimental findings; for example, at $5.5\,\mathrm{J\,cm^{-2}}$, assuming ablation occurs near the peak of the laser pulse, a calculated value of $P = 1.8 \times 10^8\,\mathrm{Pa}$, is obtained using $\gamma \cong 1.16$ [28] compared with a measured value of $\sim 8.5 \times 10^7\,\mathrm{Pa}$. Given that there is likely to be amplitude loss due to acoustic attenuation and beam expansion over the $\sim 300\,\mu\mathrm{m}$ tissue path between the tissue surface and transducer and that the model neglects fibre compression this agreement can be taken as satisfactory.

The acoustic energy radiated into the tissue during the initial high-pressure phase of the cavity expansion can be estimated as

$$\Delta E_\mathrm{A} \cong P^2 A \Delta t / \varrho c\,,$$

where A is the fibre core area, Δt the duration and P the peak pressure, respectively, of the pressure pulse. At $5.5\,\mathrm{J\,cm^{-2}}$ where $P \cong 8.5 \times 10^7\,\mathrm{Pa}$ and $\Delta t \cong 200\,\mathrm{ns}$ this corresponds to $\sim 170\,\mu\mathrm{J}$ so that only a small fraction ($\sim 2\%$) of the input energy is converted to sound in the early phase of the expansion. Unfortunately, as noted earlier, it was not possible to measure any pressure transients associated with the long time expansion and contraction phase of the bubble because of the complicating effect of acoustic reflections.

6 Discussion

It has been found that damage to a retina sample can occur with 400 ns HF-laser pulses delivered by a fibre in saline with the fibre tip positioned beyond 2 mm from this tissue. As is evident from Fig. 2, bubble growth is not fast enough to clear water between the fibre tip and sample at this range on the time scale of the laser pulse and the bubble cannot act as a transmissive cavity for the IR radiation [15, 16]. It can thus be deduced that this damage is not a direct result of laser photoablation. For the cornea this matter could not be determined from the shadowgraphs because of the small spatial scale involved so it is necessary to estimate from theoretical considerations whether water clears the intervening space. This is difficult because of the geometry but if it is assumed that fluid compressibility defines the (initial) maximum flow velocity then in the plane wave approximation the clearance time is $\sim a\varrho c/P$, where a is the fibre core radius. For $P \cong 8.5 \times 10^7\,\mathrm{Pa}$ corresponding to a fluence of $5.5\,\mathrm{J\,cm^{-2}}$ this gives $4\,\mu\mathrm{s}$ which is significantly longer than the laser pulse. Thus we suggest that even for the small distances involved for the cornea that water will remain in the vicinity of the fibre tip on the timescale of the laser pulse and attenuate the beam. This conclusion is qualitatively supported by the morphology of the damaged surface which differs significantly from that produced by direct HF-laser photoablation [14]. The appearance of the SEM for the non-contacted fibre (Fig. 5) suggests that damage has produced a separation of the collagen fibrils of the stroma of the cornea. This may be the result of pressure waves that have disrupted the normal tight packing of the fibrils. The loose fibrils have then moved forward to be above the surface of the tissue (this may be an artifact associated with tissue swelling). It is thus reasonable to deduce for both cornea and retina that either impingment of the hot vapour cavity and associated jetting effects (Fig. 4) or large amplitude acoustic waves are responsible for this. Given the relatively low energy content of acoustic waves generated in the initial expansion phase of the cavity and the lack of any clear mechanistic origin for "ablative" damage by such waves we tentatively conclude that energy transferred to the surface by the cavitation bubble is the main source of this damage. It should be noted, however, that although acoustic waves may not be instrumental in removing significant levels of material from the surface they can be damaging to tissue cells over a relatively large range when ablation takes place in a confining liquid [29] as is the case here.

The ablation rate for cornea with the contacted fibre in saline falls well below that for air [14] particularly at high fluence (e.g. at $5\,\mathrm{J\,cm^{-2}}$ this is $\sim 0.8\,\mu\mathrm{m}$ per pulse which is about ten times lower). Although at first sight this might be expected if an intervening water layer acts to block the beam from the surface as etching proceeds to greater depths, the fact that the removal rate per pulse is approximately constant with pulse number (Fig. 10) suggests this is not the case. A possible explanation for this behaviour is that gaseous ablation products (seen expanding and then contracting in the vicinity of the fibre tip in Fig. 6) remain trapped in the shallow ablation cavity and prevent water from refilling this cavity. This would then allow the beam to reach the surface without significant attenuation. The difference in ablation rates for the contacted fibre in air and in saline would then be due to the saline preventing rapid expansion of the ablation products such that they were maintained at high density and continued to attenuate the beam *during* the laser pulse. An effective attenuaton coefficient of $\sim 1.2 \times 10^4\,\mathrm{cm^{-1}}$ derived from the slope of the etch-rate line (Fig. 9) would be consistent with this interpretation in that this is close to that for the parent material [30]. The relatively smooth morphology of the irradiated site (Fig. 11) which is similar to the result for ablation in air is also supportive of removal being due to direct photoablation rather than some secondary effect.

In terms of minimizing the damage range associated with the cavitation bubble and associated acoustic transients it would be of interest to use smaller diameter fibre cores as, for example, have been used for Ho:YAG surgery [31]. The maximum bubble diameter can be estimated from (3) as

$$R_\mathrm{m} = (3\delta a^2 F / 4P_0)^{1/3},$$

where F is the fluence at the fibre tip and δ the fraction of energy that is available to support bubble growth ($\sim 5\%$ from the present experiments). For a fixed fluence R_m varies as $a^{2/3}$ so that the bubble range is reduced as the fibre core radius is decreased. In addition, the smaller effective acoustic source size would lead to a more rapid transition to three-dimensional acoustic wave expansion and hence sharper fall-

off in pressure with distance. Smaller fibres also have the advantage of improved flexibility. The penalty, however, would be lower tissue volume removal rates although this could, in principle, be offset by the use of a high repetition rate laser which could operate at low energies because of the reduced energy input needed for the fibre.

Acknowledgements. We gratefully acknowledge the technical assistance of B.L. Tait and P. Monk, and financial support from the Middlemore Award, British Medical Association. MEK is supported by a research studentship from the Iranian government.

References

1. J.T. Walsh, T.J. Flotte, T.F. Deutsch: Lasers Surg. Med. **9**, 313 (1989)
2. H. Dunbar Hoskins, A.G. Inwach, A. Vassiliadis, M.V. Drake, D.R. Hennings: Ophthalmol. **98**, 1394 (1991)
3. T. Seiler, J. Marshall, S. Rothery, J. Wollensak: Lasers in Ophthalmol. **1**, 49 (1986)
4. H. Loertscher, S. Mandelbaum, R.K. Parrish, J.M. Parel: Am. J. Ophthalmol. **102**, 217 (1986)
5. G.L. Valderrama, R.F. Menefee, B.D. Krenek, M.J. Berry, M.P. Sartori, P.D. Henry: SPIE **1202**, 149 (1990)
6. G.A. Peyman, N. Katoh: Int. Ophthalmol. **10**, 245 (1987)
7. R. Linsker, R. Srinivasan, J.J. Wynne, D.R. Alonso: Lasers Surg. Med. **4**, 201 (1984)
8. S.L. Trokel, R. Srinivasan, B. Braren: Am. J. Ophthalmol. **96**, 710 (1983)
9. D.L. Singleton, G. Paraskevopoulos, R.S. Taylor, L.A.J. Higginson: IEEE J. QE-**23**, 1772 (1987)
10. T.I. Margolis, D.A. Farnath, M. Destro, C.A. Puliafito: Arch. Ophthalmol. **107**, 424 (1989)
11. G.E. Kopchok, R.A. White, M. Tabbara, V. Saadatmanesh, S.K. Peng: Lasers Surg. Med. **10**, 405 (1990)
12. M.L. Wolbarsht: IEEE J. QE-**20**, 1427 (1984)
13. I.E. Kochevar: Lasers Surg Med. **9**, 440 (1989)
14. P.E. Dyer, M.E. Khosroshahi, S.J. Tuft: Lasers in Med. Sci. **7**, 331 (1992)
15. C.P. Lin, D. Stern, C.A. Puliafito: Invest. Ophthalmol. Vis. Sci. **31**, 2546 (1990)
16. T.G. van Leeuwen, M.J. van der Veen, R.M. Verdaasdonk, C. Borst: Lasers Surg. Med. **11**, 26 (1991)
17. R. Srinivasan, K.G. Casey, J.D. Haller: IEEE J. QE-**26**, 2279 (1990)
18. F.W. Cross, R.K. Al Dhahir, P.E. Dyer: J. Appl. Phys. **64**, 2194 (1988)
19. B. Zysset, J.G. Fujimoto, C.A. Puliafito, R. Birngruber, T.F. Deutsch: Lasers Surg. Med. **9**, 193 (1989)
20. A. Vogel, P. Schweiger, A. Frieser, M.N. Asiyo, R. Birngruber: IEEE JQ-**26**, 2240 (1990)
21. W. Lauterborn (ed.): *Cavitation and Inhomogeneities in Underwater Acoustics*, Springer Ser. Electrophys., Vol. 4 (Springer, Berlin, Heidelberg 1980)
22. F.R. Young: *Cavitation* (McGraw-Hill, Oxford 1989)
23. W. Lauterbom: General and Basic Aspects of Cavitation, In *Finite Amplitude Wave Effects in Fluids*, ed. by L. Bjorno (IPC Science & Technology Press 1974) pp. 195–202
24. P. Teng, N.S. Nishioka, W.A. Farinelli, R. Rox Anderson, T.F. Deutsch: Lasers Surg. Med. **7**, 394 (1987)
25. B.H. Flowers, E. Mendoza: *Properties of Matter* (Wiley, London 1970)
26. G.M. Hale, M.R. Querry: Appl. Opt. **12**, 555 (1973)
27. J.M. Parker, P.W. France: Properties of Fluoride Glasses. In *Fluoride Glass Optical Fibres*, ed. by P.W. France (Blackie, Glasgow 1990) Chap. 2
28. A.D. Zweig, T.F. Deutsch: Appl. Phys. B **54**, 76 (1992)
29. Y. Yashima, D.J. McAuliffe, S.L. Jacques, T.J. Flotte: Lasers Surg. Med. **11**, 62 (1991)
30. G.L. Valderrama, R.F. Menefee, B.D. Krenek, M.J. Berry: SPIE **1064**, 135 (1989)
31. S. Borirakchanyavat, C.A. Puliafito, G.H. Kliman, T.I. Margolis, E.L. Gallen: Arch. Ophthalmol. **109**, 1605 (1991)